Interfacial wetting-induced nanorheology of thin polymer films

Haiyang Zhang,[1,*] Quanyin Xu,[1,*] Weilong Gong,[1] Shasha Liu,[2] Jintian Luo,[1,†] Rodney D. Priestley,[2] and Biao Zuo[1,‡]

[1]*School of Chemistry and Chemical Engineering, Key Laboratory of Surface & Interface Science of Polymer Materials of Zhejiang Province, Zhejiang Sci-Tech University, Hangzhou 310018, China*

[2]*Department of Chemical and Biological Engineering, Princeton Materials Institute, Princeton University, Princeton, New Jersey 08544, USA*

(Received 20 April 2024; revised 11 October 2024; accepted 15 May 2025; published 4 June 2025)

The rheological response and chain dynamics of thin polymer films underpin nanoscale polymer processing, yet molecular confinement alters such behavior. Using the interfacial wetting force of an immiscible liquid droplet to deform the films and linear elastic theory to describe the time evolution of the deformation profile, we demonstrated that the linear viscoelastic spectra, i.e., the frequency-dependent storage and loss moduli, of nanoscale polymer films are experimentally accessible over a wide frequency range. Our measurements on polystyrene nanofilms evidence an acceleration of polymer diffusion at a large confining length scale, i.e., at film thicknesses of hundreds of nanometers. This long-range perturbation in chain dynamics was interpreted as the fast relaxation of surface chains with reduced entanglements provoking loosening of entanglement constraints of the underlying chains, allowing the accelerated reptation mobility at the surface to extend deeply into the film interior. This suggests a surface-induced constraint release effect dominating the dynamics and rheology of polymers confined at a large length scale.

DOI: 10.1103/PhysRevResearch.7.023226

I. INTRODUCTION

Advances in modern technology rely on the ability to fabricate sophisticated nanostructures that require fine control of rheological behavior of materials when confined at various length scales. The rheological response and dynamics of thin polymer films determine the means and conditions for fabricating stable nanostructures with diverse morphologies [1–3]. Since the early 1990s, the dynamics of confined polymers have been explored to better understand the molecular behavior of nanomaterials [4–11]. The glass transition temperature (T_g), which is associated with segmental relaxation, is depressed in supported and freestanding films with thicknesses $<$100 nm [12–17]; the rubbery response, pertinent to the relaxation of entanglement strands, stiffens by increasing the plateau modulus in both entangled and unentangled polymer films [18–20]. The terminal relaxation of entangled chains speeds up in thin films with a thickness of $\sim$10 R_g [21–24], whereas large-strain squeeze flow increases in highly confined films thinner than the coil size [25]. These observations of changes in segment and chain dynamics due to confinement at different sizes suggest that polymer dynamics at different length scales may not be equally sensitive to confinement. This presents challenges in building a consistent image of the dynamics of confined polymers because the glass transition and rubbery and terminal responses at different parts of the time spectra identified by various experiments appear to be incompatible with each other in the framework of existing theories. This continues to inspire the need to develop technologies to assess global spectra of relaxation times to comprehend the unusual dynamic properties of confined polymers.

The linear viscoelastic (LVE) spectrum, based on the frequency-dependent storage and loss moduli [$G'(\omega)$ and $G''(\omega)$, respectively], which carries information about most relaxation processes, allows the assessment of global dynamics over multiple molecular length scales spanning a wide time domain from the glass transition to the terminal zone [26,27]. Although broad LVE spectra have been measured for bulk polymers using standard rheometers that directly generate $G'(\omega)$ and $G''(\omega)$ [28], the LVE spectra of thin polymer films, particularly nanoscale films coated on solid substrates, are difficult to obtain [29]. Based on our previous findings of surface creep as a result of interfacial wetting [30], and inspired by the investigations using liquid capillarity to assess polymer dynamics [31–34], we developed a thin-film nanorheology technique which generates the $G'(\omega)$ and $G''(\omega)$ of polymer films on solid substrates by monitoring the time evolution of ridgelike deformations, called "wetting ridges," generated by wetting of a liquid droplet on the film surface. This paper describes the measurement and analysis of the wetting ridges, validates the proposed approach using 600 nm thick films as confinement-free models, and importantly, we

*These authors contributed equally to this work.
†Contact author: luojt@zstu.edu.cn
‡Contact author: chemizuo@zstu.edu.cn

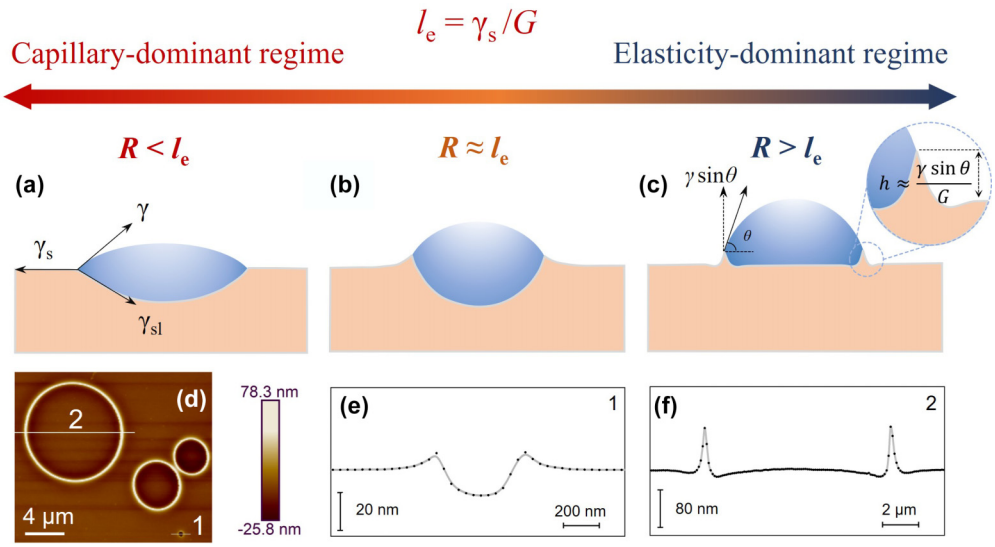

FIG. 1. Illustration of the elastocapillary deformation. Panels (a)–(c) show substrate-droplet configurations in the capillary-dominant ($R < l_e$), capillary-to-elasticity transition ($R \sim l_e$), and elasticity-dominant ($R > l_e$) regimes, respectively. (d) AFM image showing deformations caused by droplets of different sizes on the surface of a 600 nm thick PS film with a molecular weight of 282 kg/mol (PS282k); (e), (f) cross-sectional AFM profiles of surface deformations marked by 1 and 2 in panel (d). Specifically, deformations were formed at $T_g + 15\,^{\circ}C$ by depositing droplets of various radii on the film surfaces, and AFM images were acquired after quenching the films and removing the droplets.

investigate the effect of confinement on the viscoelastic relaxation of PS films with thicknesses down to 50 nm. We observed the acceleration of polymer relaxation upon confinement in the submicron thick polymer films, and demonstrate that the confinement-induced variations in chain dynamics can be consistently represented using the tube-reptation model with an additional surface-evoked constraint release effect. This suggests that both confined and unconfined polymer motions have a common molecular basis, namely, chain reptation; however, confined polymers experience additional effects such as a decrease in T_g, a decrease in entanglement, and a long-range constraint release effect emanating from the surface, as demonstrated in this study.

II. MATERIALS AND METHODS

A. Materials

Monodisperse polymers of polystyrene (PS), poly(4-methylstyrene) (P4MS), poly(4-tert-butylstyrene) (PtBS), and poly(α-methylstyrene) (PαMS) were purchased from Polymer Source, and used as received; see the details of physical characteristics in Table S1 in the Supplemental Material [35]. The ionic liquid (IL), 1-ethyl-3-methylimidazolium tetrafluoroborate ([EMIM]BF_4), with a surface tension of 49 mN/m and a negligible vapor pressure, purchased from Sigma-Aldrich (Table S2 [35]), was used as the test liquid.

B. Preparation of polymer films

Toluene solutions of polymers were spin coated onto a silicon wafer covered by a 2.2 nm naturally oxidized layer to form films with various thicknesses. The thickness of the films was determined by a spectroscopic ellipsometer (RC2 from J. A. Woollam, USA). The films were then annealed at 50 °C above T_g for 72 h under vacuum to remove any residual solvents and stresses. The T_g values of the polymer films were determined by a heating scanning at a rate of 5 °C/min on the ellipsometer.

C. Formation and characterization of the wetting ridge on film surface

We used an *ex situ* method to assess the surface deformation of films induced by the [EMIM]BF_4 droplets sitting on viscoelastic PS films for various time [36]. In the experiment, polymer films of PS, PtBS, P4MS, or PαMS on Si wafers were mounted on a hot stage that was preheated above the respective T_g of the polymers. Two methods were used to deposit IL droplets onto the surface of the films. A nebulization-deposition method (i.e., the IL microdroplets were nebulized through a Venturi nozzle and slowly deposited onto the film surface by gravity [36]) was used to generate microdroplets with radius (R) ranging from 0.1 to tens of micrometers to investigate the elastocapillary deformation of the polymer films as a function of the R or, namely, to acquire the atomic force microscopy (AFM) images shown in Fig. 1(d). Meanwhile, to assess the time evolution of the wetting ridge and to investigate the viscoelastic creep of polymer films, a large droplet with a volume of 3 μL and a radius of 1.3 mm, which ensures that $R \gg l_e$ (l_e: elastocapillary length) and the deformation is determined by the polymer mechanics, was deposited on the film surface using an injection syringe; Fig. S1 [35] shows the configuration of the droplet on the polymer film surfaces.

After deposition, the films with droplets atop were covered with a transparent glass dome to prevent interference of the external environment. After a time t for the wetting ridge beneath the drop to develop and grow, the films with the droplets atop were quenched to freeze the surface ridge by transferring the hot films onto a cold copper surface. The

IL droplets on the film surfaces were then washed off using de-ionized water. The morphology of the exposed ridges was visualized using atomic force microscopy (AFM, ICON from Bruker, USA) in the tapping mode at room temperature. The AFM images were processed using NanoScope Analysis software to extract the two-dimensional (2D) cross-sectional profiles of the ridges.

By varying the droplet placement time t and repeating the measurements as described above, the time evolution of the wetting ridge profile can be assessed.

D. Rheological tests of bulk polymers

The linear viscoelastic (LVE) spectra of the bulk polymers were characterized by a small-amplitude oscillatory shear on a stress-controlled rheometer (MARS60 from HAAKE, Thermo-Scientific, Germany), equipped with 8 mm parallel plates. Samples were molded at $T_g + 30\,^{\circ}\mathrm{C}$ to form disks of 8 mm diameter and about 1 mm thickness to match the geometry. Frequency sweep tests were performed at a constant stress of 0.2 kPa within the linear viscoelastic region at various temperatures. Then, time-temperature superposition (TTS) was applied to construct master curves for each sample at selected reference temperatures.

III. RESULTS AND DISCUSSION

A. Liquid wetting-induced film deformation

Our approach is based on partial wetting-induced elastocapillary deformation [36–39]. When a liquid droplet rests on a soft solid, the underlying material is deformed by the sessile droplet [37–41]. When the droplet radius (R) $< l_e$ (l_e: the elastocapillary lengthl $l_e \approx \gamma_s/G$, where γ_s is the surface tension and G is the elastic modulus of the solid), the deformation is determined by the balance among three interfacial tensions at the three-phase contact line to adopt the droplet as a floating liquid lens [Fig. 1(a)]. Conversely, if $R > l_e$ (in the elasticity-dominant regime), the substrate elasticity determines the deformation. In the latter case, the substrate is not affected by the droplet, except for a local region near the contact lines [Figs. 1(c), 1(d), and 1(f)]. In this region, the upward component of the droplet surface tension ($\gamma \sin\theta$) is balanced by the elastic stress of the substrate, resulting in the formation of a wetting ridge with the height (h) determined by the substrate elastic modulus [42–44]. In the intermediate case ($R \sim l_e$), the droplet-substrate shape is characterized by a deep indentation beneath the droplet surrounded by a circular hump along the contact line [Figs. 1(b), 1(d), and 1(e)] owing to the coupled effect of the elasticity and capillarity of the substrate. The surface deformation caused by liquid wetting provides an opportunity to investigate the mechanical relaxation of polymer films by analyzing the time evolution of the wetting ridge in the elasticity-dominant regime.

B. Nanorheological measurement on the nanofilms

We used hydrophobic monodisperse PS and its derivatives, P4MS, PtBS, and PαMS, as model polymers (see the physical characteristics of these polymers in Table S1 of the Supplemental Material [35]) and the hydrophilic IL of [EMIM]BF_4 as the test liquid (Table S2 [35]). The nonvolatile [EMIM]BF_4 partially wetted the PS, PtBS, P4MS, and PαMS films, forming stable contact angles of $72^{\circ}-88^{\circ}$, which were constant over time (Fig. S1 in the Supplemental Material [35]). Notably, the polymers were immiscible with [EMIM]BF_4; the T_g values remained constant after mixing with the IL (Fig. S2 [35]), demonstrating that the IL had no swelling or plasticizing effect on the polymers. In the experiment, a large IL droplet of 3 μL in volume and 1.3 mm in radius ($R \gg l_e = 0.1 - 0.4$ μm, Table S1 [35]) was deposited on the surface of a supported polymer film mounted on a heating stage at $T > T_g$ to generate a wetting ridge in the elasticity-dominant regime.

Figure 2(a) shows the AFM morphologies of the wetting ridges formed at different droplet resting times t. The surface ridge displayed the most substantial deformation at a horizontal position of $x = 0$ and underwent a gradual decline along the x axis before reaching the flat region, Fig. 2(b). The well-defined ridge profile, $H(x)$, was generated by minimizing the total free energy, which includes the elastic energy of polymer deformation and the surface energy relevant to the film surface elevation [45]. $H(x)$ can be described by a linear elastic model proposed by Jerison *et al.* [44] and Style and Dufresne [46]:

$$H(x) = hf_d(x) = \frac{\gamma \sin\theta}{2\pi G}\int_0^{\infty} \frac{\cos sx\, \mathrm{d}s}{s\left(\frac{1+2s^2+\cosh 2s}{-2s+\sinh 2s} + \frac{\chi s}{2}\right)}, \quad (1)$$

where s is the reciprocal variable of x based on the Hankel transformation and $\chi = \gamma_s J/d$ (d is the film thickness). Equation (1) demonstrates that, in addition to the film thickness and liquid surface tension, $H(x)$ is determined by the elastic modulus (G) or compliance (J; $G = 1/J$) of the solid. By fitting the experimental ridge profiles in Fig. 2(c) at various t using the numerical solution of Eq. (1), the fitting parameter, $J(t)$, describing the polymer creep can be elucidated. Remarkably, the $J(t)$ was quantitatively consistent with that obtained using the shear rheometer (Fig. S3 [35]), suggesting that the rise and broadening of the ridge over time is explicitly related to the increase in creep compliance caused by viscoelastic relaxation of the polymer.

Notably, a solution to Eq. (1) at $x = 0$ provides a succinct relationship:

$$h = \frac{k\gamma \sin\theta}{G} = k\gamma \sin\theta J, \ \text{at } x = 0. \quad (2)$$

where k is a geometrical factor that is independent of the polymer dynamics (see Eq. (S1) [35] for the expression of k). This relationship indicates that the time dependence of the ridge height, $h(t)$, provides an appropriate representation of the creep of polymer films, $h(t) = k\gamma \sin\theta J(t)$. Additionally, the stress generated by the surface tension (<0.08 MPa) was much smaller than the yield stress of the polymers ($\sim 10^1$ MPa), confirming a linear viscoelastic response of the films induced by the liquid capillarity.

To further verify the relationship between $h(t)$ and $J(t)$, as well as the polymer dynamics, we superposed the $h(t)$ curves of PS282k measured at different temperatures to generate a master curve [Fig. 3(a)] by horizontally shifting the $h(t)$ curves using shift factors ($a_{T,W}$) according to a reference temperature (T_{ref}) (see Fig. S4 [35] for the other polymers).

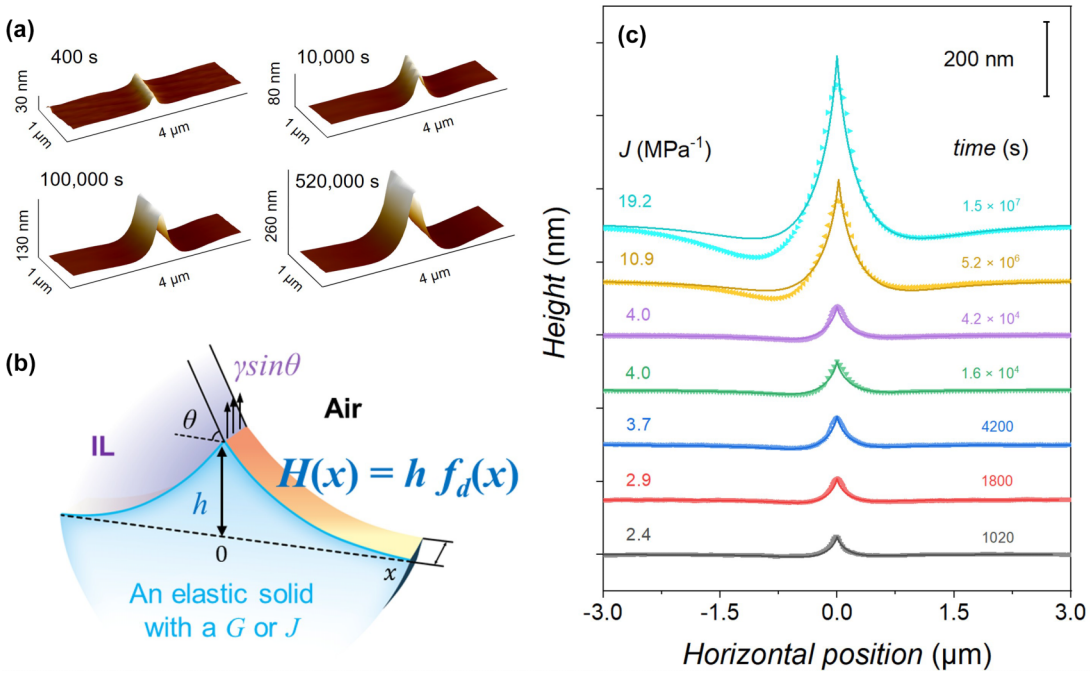

FIG. 2. Time evolution of wetting ridge profiles. (a) Three-dimensional AFM images of wetting ridges formed on 600 nm thick PS282k films at 105 °C for various t. (b) Illustration of a typical $H(x)$ profile on an elastic solid, described by $H(x) = hf_d(x)$, in which h describes the height of the wetting ridge and $f_d(x)$ delineates how the surface deformation decays to become flat. (c) AFM cross-sectional profiles of wetting ridges on PS282k films formed at various t; the solid curves are the fitting results using Eq. (1) to obtain the $J(t)$.

The master curves of all the polymers showed a plateau region at the intermediate timescale, before and after which the ridges grew with time. The plateau was ascribed to the transient entanglement network formed among the polymers, which, according to the linear viscoelasticity of polymers, prevented the chain molecules from diffusing and macroscopically flowing [26,27]. In particular, for PS282k, the $a_{T,W}$ values, which reflect the growth kinetics of the wetting ridges, were consistent with the shift factor (a_T) describing the polymer dynamics obtained using small-amplitude oscillatory shear tests on a standard rheometer [Fig. 3(b)]. The temperature dependence of $a_{T,W}$ can be described by the Williams-Landel-Ferry (WLF) equation [47] (Fig. 3(b) and S5 [35]), and the dynamic fragility (m) derived from fitting the parameters of C_1 and C_2 was consistent with the values obtained using standard techniques (Table S3 [35]). The good alignment between the ridge growth kinetics and the polymer dynamics suggests that the $h(t)$ master curves represent the polymer creep at T_{ref} over a broad time range.

Based on the relationship of $h(t) = k\gamma \sin\theta J(t)$, the $h(t)$ can be converted to the dynamic compliance $[J^*(\omega)]$ of the viscoelastic polymers in the unilateral Fourier frequency

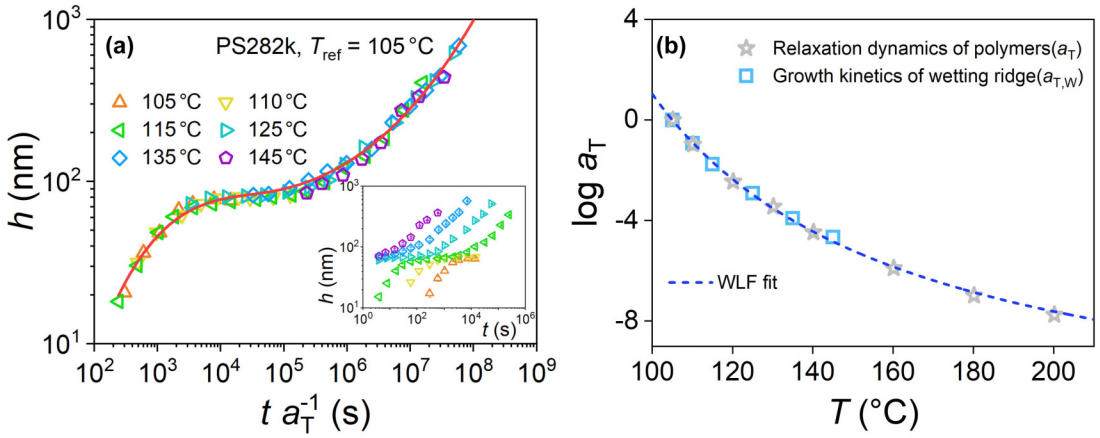

FIG. 3. Growth of wetting ridge and polymer dynamics. (a) Master curve of $h(t)$ at T_{ref} obtained by shifting the $h(t)$ curves at various temperatures shown in the inset. The solid red curve represents cubic B-spline interpolation for smoothing the master curve, from which the $\alpha(\omega)$ values in Eq. (5) are derived. (b) Temperature dependence of $a_{T,W}$ and a_T for PS, derived from the growth kinetics of the wetting ridges and measured using a standard rheometer, respectively.

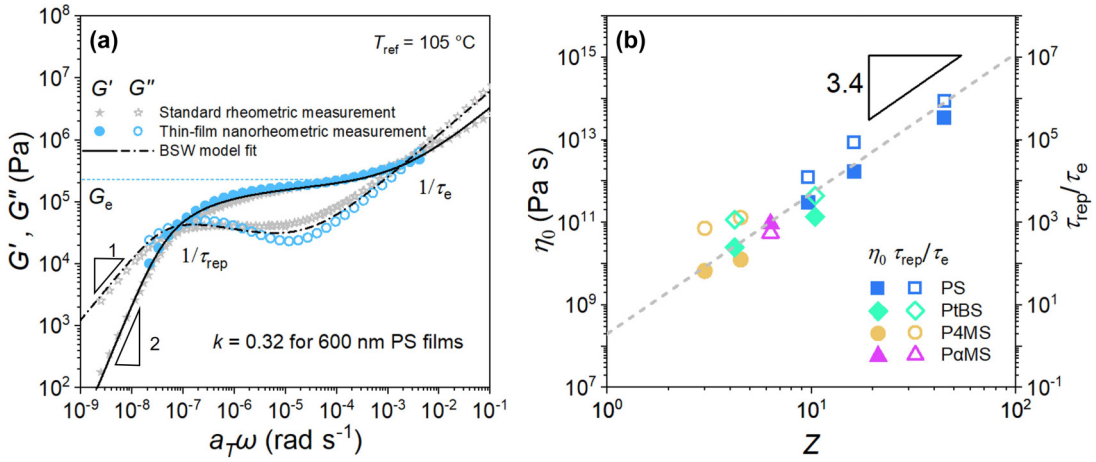

FIG. 4. Linear viscoelasticity of PS films. (a) LVE spectra for the 600 nm thick PS282k film. The blue circles and gray stars represent G' and G'' obtained using the nanorheology approach and a standard rheometer, respectively. The solid and dashed-dotted curves show the results of the Baumgaertel-Schausberger-Winter (BSW) fits [51] of the $G'(\omega)$ and $G''(\omega)$ data according to Eq. (S9) [35]. (b) Relationships of $\tau_{rep}/\tau_e \sim Z^{3.4}$ and $\eta_0 \sim Z^{3.4}$ for films of PS and PS derivatives ($d = 600$ nm).

domain [48]:

$$i\omega\mathcal{F}_u[h(t)] = k\gamma \sin\theta J^*(\omega), \tag{3}$$

where $\mathcal{F}_u[h(t)]$ is the unilateral Fourier transform of $h(t)$. Then the dynamic modulus, $G^*(\omega)$, is given by [48]

$$G^*(\omega) = \frac{1}{J^*(\omega)} = \frac{k\gamma \sin\theta}{i\omega\mathcal{F}_u[h(t)]}. \tag{4}$$

We used an algebraic method proposed by Mason [49] to estimate $\mathcal{F}_u[h(t)]$, which expands $h(t)$ locally around the frequency ω ($t = 1/\omega$) as a power law, i.e., $h(t) \approx h(1/\omega)[(\omega t)^{\alpha(\omega)}]$, and thus

$$\begin{aligned}\mathcal{F}_u[h(t)] &\approx \int_0^\infty h\left(\frac{1}{\omega}\right)(\omega t)^{\alpha(\omega)} e^{-i\omega t} dt \\ &= \frac{h(1/\omega)\Gamma[1+\alpha(\omega)]}{\omega} e^{-\frac{i\pi[1+\alpha(\omega)]}{2}},\end{aligned} \tag{5}$$

where $\Gamma[\cdots]$ is the gamma function [50] and $\alpha(\omega) = (d\log h/d\log t)_{t=1/\omega}$ is obtained as the derivative of the logarithmic $h(t)$ curve interpolated via cubic B-spline regression [i.e., the red curve in Fig. 3(a)]. Equation (5) was effective for calculating $\mathcal{F}_u[h(t)]$, because the α value at every $\omega = 1/t$ can be accurately determined based on the interpolated smooth $h(t)$ curves; see the red solid curve in Fig. 3(a).

By combining Eqs. (4) and (5), $G'(\omega)$ and $G''(\omega)$ were determined as the real and imaginary parts of the dynamic modulus, respectively, i.e., $G^*(\omega) = G'(\omega) + iG''(\omega)$, using the $h(t)$ master curves. Figures 4(a) and S6 [35] show the $G'(\omega)$ and $G''(\omega)$ of PS282k and the other polymers at theirT_{ref}'s. Notably, the LVE spectrum of PS282k overlapped almost completely with that measured using a standard rheometer, confirming the validity and accuracy of our approach. The frequency at which G' exceeds G'' signifies the Rouse relaxation time of entanglement strands (i.e., τ_e), and that where G'' exceeds G' indicates the onset of the flow of the polymer chains by reptation across the entanglement tube (i.e., the reptation time, τ_{rep}) [27]. The τ_e and τ_{rep} values identified from our LVE spectra are listed in Table S4 [35].

The complex viscosities of the films were determined as $|\eta^*| = (G'^2 + G''^2)^{1/2}/\omega$, of which the low-frequency asymptotic value identifies the zero-shear viscosity (η_0) [48], (Fig. S7 [35]). We plotted η_0 and τ_{rep}/τ_e against the number of entanglements in a chain ($Z = M_w/M_e$, where M_e is the entanglement molecular weight) at a log-log scale [Fig. 4(b)]. A linear relationship with a slope of 3.4 is evident, i.e., $\tau_{rep}/\tau_e \sim Z^{3.4}$ and $\eta_0 \sim Z^{3.4}$, which was consistent with the polymer rheology and tube-reptation model [52–54]. Overall, the interfacial wetting experiments, analysis, and modeling of the resultant surface deformations provide a method to capture the rheology and dynamics of supported polymer films with varying thicknesses.

C. Submicron confinement accelerates polymer diffusion

This approach was used to investigate the dynamics of confined polymers while reducing the film thickness to that approaching the coil dimensions of the chains. Figure 5(a) show the LVE spectrum of PS films with various thicknesses. It is apparent that reducing the thickness of the PS282k films to <300 nm resulted in an almost unchanged τ_e and a monotonously decreasing τ_{rep}, accompanied by a progressive shortening of the rubbery plateau; see Fig. 5(b). The reduced τ_{rep} and shrunken plateau breadth (i.e., reduced in τ_{rep}/τ_e) indicate the ease of polymer diffusion in thin films, which is consistent with previous observations of reduced viscosity [21,22] and terminal relaxation time [23], as well as the increased M_e of polymers in confined environments. Normalizing τ_{rep}/τ_e of the thin films to their bulk values (λ_{bulk}; $\lambda_{bulk} = \tau_{rep,bulk}/\tau_{e,bulk}$), as well as the thickness to the R_g or end-to-end distance (R_{EE}) of the polymers, the data for PS with various M_w were superposed into a single curve [Fig. 5(b)], evidencing a universal chain dimension-relevant confinement effect.

Notably, the critical thickness, identified in the LVE spectra, corresponding to the changeover to where the film is in a confined regime, in which the chain diffusion is accelerated and the rubbery plateau is shortened, was in the submicron

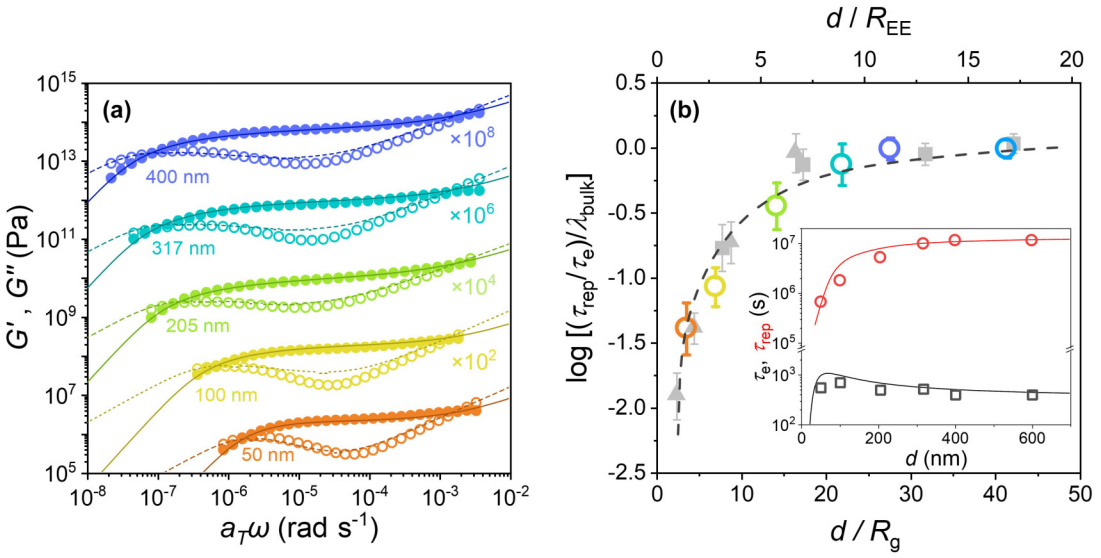

FIG. 5. Acceleration of polymer dynamics under submicron confinement. (a) $G'(\omega)$ and $G''(\omega)$ of PS282k films of various thicknesses at $T_{ref} = 105\,^{\circ}$C (the original $h(t)$ curves are shown in Fig. S8 [35]). The data are vertically shifted for clarity, and the solid and dashed curves represent the BSW fitting results. (b) Thickness dependence of $(\tau_{rep}/\tau_e)/\lambda_{bulk}$ for PS films with M_w of 282 (empty circles), 168 (gray squares), and 780 (gray triangles) kg/mol. The inset shows the τ_{rep} and τ_e values for the PS282 film. The dashed and solid curves in the main panel and the inset, respectively, represent the results predicted by the double reptation model in thin films. LVE spectra of thin PS films with $M_w = 168$ and 780 kg/mol are shown in Fig. S8 [35].

range (i.e., ∼300 nm) and approximately 20 times the R_g of PS. The critical confinement size for the linear dynamics appears to be larger than that for the nonlinear squeeze flow, in which the chain diffusion is faster only when the film thickness is reduced to a scale comparable to the chain size, where the polymer coils are severely compressed [25]. Of relevance to our experiment, Bodiguel and Fretigny observed a reduction of viscosity in the linear regime in a similarly thick PS film (300–400 nm, corresponding to 9–12 R_g) [21]. The results of linear rheology of polymer films imply that the motion of entangled, high-molecular-weight chains are accelerated by confinement at the submicron length scale. This confinement scale (i.e., submicron) for polymer diffusion is much larger than that for T_g and cooperative segmental motion in PS films, which is typically less than 100 nm [55–58], suggesting a unique mechanism beyond the T_g shift by which chain diffusion is speed up in the submicron thick films with a thickness of tens of polymer R_g.

D. Surface-induced constraint release (SICR) effect

The entangled polymer diffusion is realized by chain slithering within a virtual tube [53] (i.e., reptation; see Fig. 6). Herein, we explain the submicron confinement effect and long-range effect on chain diffusion by a rapid surface relaxation-induced release of entanglement constraints in thin films. This effect emerges from the confluence of the surface effect, which reduces entanglement (i.e., increases the M_e; $M_{e,surface} \approx 3 \sim 4\ M_{e,bulk}$) [59–62] and accelerates reptation of the surface chain due to the reduced primitive contour length, and the constraint release effect, which facilitates polymer relaxation by releasing the entanglement constraints of the polymers through movement of their surrounding chains. As illustrated in Fig. 6, as the fast-reptating surface chain moves away, the topological constraints that were once imposed on the underlying chains are released, thereby accelerating chain relaxation underneath the surface coils. That is, *the activation of surface reptation dynamics has a knock-on effect on its neighborhood*, essentially loosening the topological constraints on the adjacent chains below and allowing them to diffuse as though they are affected by the presence of a free surface. Such dynamical facilitation could propagate over a distance larger than the chain dimension because of the strong intrachain interactions of the entangled polymers, leading to a perturbation of the chain dynamics upon confinement at large length scales that exceed 100 nm and can be normalized by the chain dimension R_{EE}, i.e., d/R_{EE} [Fig. 5(b)].

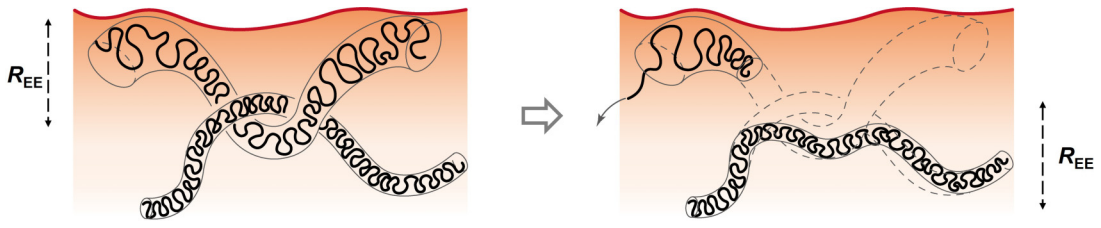

FIG. 6. Schematical illustration of SICR effect. The process of the release of entanglement constraints near the polymer surfaces.

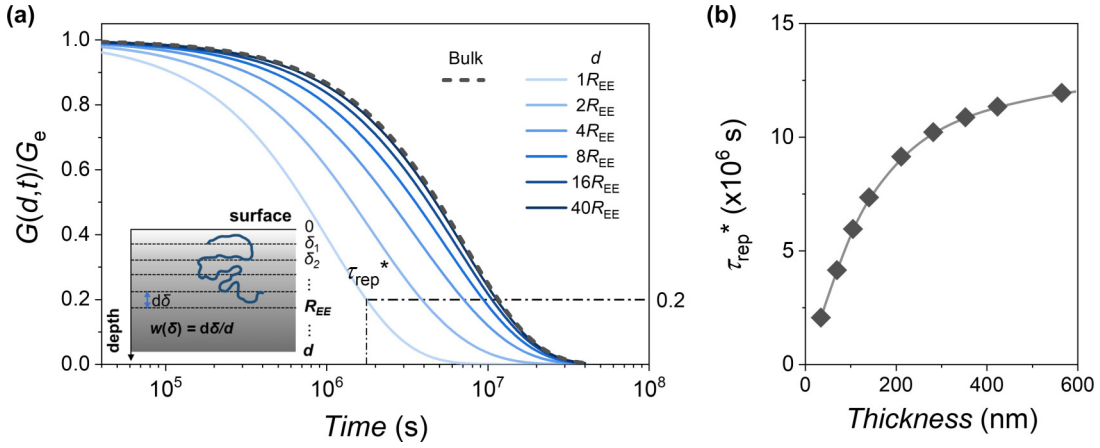

FIG. 7. Chain dynamics predicted by the double reptation model for thin films. (a) Simulated stress relaxation curves of PS film with various thicknesses using bulk τ_e and $M_e(\delta)$. The inset shows the schematic representation of the continuous multilayer structure employed to describe the $M_e(\delta)$. (b) Thickness dependence of the τ^*_{rep}.

The process of constraint release is very complex, and it is still lacking a fully generalized, rigorous theory. Here, we sought to use the "double reptation" theory [56]—a simple description of constraint release effect on the relaxation of polydisperse polymers—to account for the SICR effect and to describe the chain relaxation in $20R_g$-thick PS films. The double reptation model describes the acceleration of reptation of long polymer chains due to the constraint release induced by interaction with fast-relaxing short chains. The relaxation modulus, $G(t)$, of the polydisperse polymer consisting of n components at a time t is given by [56]

$$\frac{G(t)}{G_e} = \left[\sum_n w_n P(t, Z_n)\right]^2. \tag{6}$$

The subscript n denotes the component chains with the primitive length Z_n, and w_n is the weight fraction of each component polymer. $P(t, Z_n)$ is the tube survival probability of the n chains at time t—the fraction of the tube that remains confining the chain molecule, which is 1 for the initial condition that the chain is entirely trapped in the tube, and is 0 when the chain is fully escaped from the tube. $P(t, Z_n)$ can be approximated as an exponential decay, $\exp[-t/\tau_{df}(Z_n)]$, where $\tau_{df}(Z_n)$ is the relaxation time of the n chains. $\tau_{df}(Z_n)$ is expressed as

$$\tau_{df}(Z) = 3\tau_e Z^3\left[1 - \frac{2D_1}{\sqrt{Z}} + \frac{D_2}{Z} - \frac{D_3}{\sqrt[3]{Z}}\right], \tag{7}$$

in which $D_1 = 1.69$, $D_2 = 4.17$, and $D_3 = 1.55$ [57]; the Rouse relaxation time of the entanglement strands (τ_e) can be determined by $\tau_e = \tau_0 N_e^2$ [26,57].

As for thin films of monodisperse polymers, investigated in this work, the constraint release effect is due to the presence of a mobile surface region, in which surface $M_e \approx 3 \sim 4\, M_{e,bulk}$ and the M_e decreases with the distance from the surface before recovering to the bulk value at a depth of $\delta \sim R_{EE}$; [$M_e(\delta)$; δ represents the distance from the surface] [60,61,63]. The inhomogeneity in $M_e(\delta)$ near the surface is described by a continuous multilayer model [64]; see the inset of Fig. 7(a). This leads to a depth dependence of the primitive length (Z) of the chain strands according to $Z(\delta)/Z_{bulk} = M_{e,bulk}/M_e(\delta)$, as well as the depth-dependent relaxation time, $\tau_{df}[Z(\delta)]$, defined by Eq. (7). The weight fraction, $w(\delta)$, of the strands in an individual layer at depth δ is related to the layer thickness $d(\delta)$ and the film thickness by $w(\delta) = d(\delta)/d$; see the inset of Fig. 7(a). Thus the double reptation model, i.e., Eq. (7), is modified to describe the SICR effect in thin films by integrating the contribution of each dynamically distinct layer, i.e., $w(\delta)$ and $\tau_{df}[Z(\delta)]$, to the modulus relaxation of the entire film:

$$\frac{G(d,t)}{G_e} = \left[\sum_n w_n P(t, Z_n)\right]^2 = \left[\int_0^d \frac{d\delta}{d} P[t, Z(\delta)]\right]^2 = \left[\int_0^d \frac{d\delta}{d} \exp\left(-\frac{t}{\tau_{df}[Z(\delta)]}\right)\right]^2. \tag{8}$$

Equation (8) accounts for the role of the rapidly reptating surface chains due to increasing in $M_e(\delta)$ in the stress relaxation of the polymer films due to dynamic facilitation by the SICR process. In 2005, Dalnoki-Veress and co-workers [61] reported the thickness dependence of chain entanglement and $M_e(\delta)$ of PS films by observation of the maximum extension ratio of the films; see the $M_e(\delta)$ of PS in Fig. S10 [35]. Therefore, by substituting the $M_e(\delta)$ (Eq. (S10) [35]) into Eq. (8), and keeping τ_e at the bulk value, stress relaxation of PS films, facilitated by the SICR effect, can be computed; see Fig. 7(a). Figure 7(a) describes the terminal relaxation of the PS in thin films. By defining the effective terminal relaxation time, τ^*_{rep}, as the time at which the stress relaxation function decays to 0.2, the thickness dependence of the τ^*_{rep} was obtained; see Fig. 7(a). Apparently, the τ^*_{rep} starts to decrease at $d \approx 300-400$ nm. That is, the modeling reproduces the submicron confinement effect observed in the nanorheological measurement.

Finally, we showed that by considering both the SICR effect and the confinement-induced T_g shift [12], the τ_e and τ_{rep} of PS films can be evaluated quantitatively. Section 11 of the Supplemental Material [35] describes the details of evaluation of the values of τ_e and τ_{rep} from τ^*_{rep}, T_g, and $M_e(\delta)$ of PS films. As shown in the solid and dashed curves in Fig. 5(b) and its inset, prediction of τ_e, τ_{rep}, and τ_{rep}/τ_e of the

PS films overlaps with the results obtained from the nanorheological measurements. This consistency suggests that double reptation in thin films effectively captures, with reasonable simplicity, the essential physics of the SICR effect, supporting the proposed mechanism that the rapid relaxation of surface chains releases the entanglement constraints of the underlying chains, facilitating the relaxation of polymer films at thicknesses well beyond R_g and on the submicron length scale.

IV. CONCLUSION

Using the molecular wetting force to deform films and evaluate polymer creep, we demonstrate that broad linear viscoelastic spectra of supported nanoscale thin polymer films with relaxation times spanning five orders of magnitudes are now within reach. The rheology spectra of PS films thinner than ~300 nm and ~$20R_g$ feature a shortened rubbery plateau and decreased reptation time, indicating faster chain dynamics at a large confinement length scale. The confinement effect in the submicron thick films hints at a surface-induced constraint release (SICR) mechanism; that is, the rapid reptation of the surface polymers with increasing M_e allows for partial release of the topological constraints of the underlying chains, which accelerates chain relaxation in the film interior. We showed that a double reptation model in thin films, combined with a reasonable description of surface M_e, can quantitatively estimate the SICR effect on polymer film relaxation, providing a physical insight that the increase of surface M_e can lead to an acceleration of chain diffusion over submicron distances via the SICR processes. Therefore, our study enables alternative ways to investigate and understand polymer dynamics under confinement, which could benefit polymer engineers in producing high-quality microparts by optimizing the molding processes to be compatible with the confined polymer rheology.

ACKNOWLEDGMENTS

B.Z. and J.L. acknowledge support by the National Natural Science Foundation of China (Grants No. 22122306, No. 22303084, and No. 52373025). R.D.P. acknowledges support by the National Science Foundation (NSF) Materials Research Science and Engineering Center Program through the Princeton Center for Complex Materials (PCCM) (Grant No. DMR-2011750) and the NSF via CBET Grant No. 2208260.

[1] J. Xu, S. Wang, G.-J. N. Wang, C. Zhu, S. Luo, L. Jin, X. Gu, S. Chen, V. R. Feig, J. W. F. To, S. Rondeau-Gagné, J. Park, B. C. Schroeder, C. Lu, J. Y. Oh, Y. Wang, Y.-H. Kim, H. Yan, R. Sinclair, D. Zhou *et al.*, Highly stretchable polymer semiconductor films through the nanoconfinement effect, Science **355**, 59 (2017).

[2] S. R. Forrest, The path to ubiquitous and low-cost organic electronic appliances on plastic, Nature (London) **428**, 911 (2004).

[3] Y. Yang, H. Tian, S. Napolitano, and B. Zuo, Crystallization in thin films of polymer glasses: The role of free surfaces, solid interfaces and their competition, Prog. Polym. Sci. **144**, 101725 (2023).

[4] C. L. Jackson and G. B. McKenna, The glass transition of organic liquids confined to small pores, J. Non-Crystall. Solids **131–133**, 221 (1991).

[5] G. B. McKenna, Ten (or More) years of dynamics in confinement: Perspectives for 2010, Eur. Phys. J. Spec. Top. **189**, 285 (2010).

[6] M. D. Ediger and J. A. Forrest, Dynamics near free surfaces and the glass transition in thin polymer films: A view to the future, Macromolecules **47**, 471 (2014).

[7] S. Napolitano, E. Glynos, and N. B. Tito, Glass transition of polymers in bulk, confined geometries, and near interfaces, Rep. Prog. Phys. **80**, 036602 (2017).

[8] Y. Cang, A. N. Reuss, J. Lee, J. Yan, J. Zhang, E. Alonso-Redondo, R. Sainidou, P. Rembert, K. Matyjaszewski, M. R. Bockstaller, and G. Fytas, Thermomechanical properties and glass dynamics of polymer-tethered colloidal particles and films, Macromolecules **50**, 8658 (2017).

[9] H. Kim, Y. Cang, E. Kang, B. Graczykowski, M. Secchi, M. Montagna, R. D. Priestley, E. M. Furst, and G. Fytas, Direct observation of polymer surface mobility via nanoparticle vibrations, Nat. Commun. **9**, 2918 (2018).

[10] H. Tian, Q. Xu, H. Zhang, R. D. Priestley, and B. Zuo, Surface dynamics of glasses, Appl. Phys. Rev. **9**, 011316 (2022).

[11] H. Tian, J. Luo, Q. Tang, H. Zha, R. D. Priestley, W. Hu, and B. Zuo, Intramolecular dynamic coupling slows surface relaxation of polymer glasses, Nat. Commun. **15**, 6082 (2024).

[12] J. L. Keddie, R. A. L. Jones, and R. A. Cory, Size-dependent depression of the glass transition temperature in polymer films, Europhys. Lett. **27**, 59 (1994).

[13] J. A. Forrest, K. Dalnoki-Veress, J. R. Stevens, and J. R. Dutcher, Effect of free surfaces on the glass transition temperature of thin polymer films, Phys. Rev. Lett. **77**, 2002 (1996).

[14] J. A. Forrest, K. Dalnoki-Veress, and J. R. Dutcher, Interface and chain confinement effects on the glass transition temperature of thin polymer films, Phys. Rev. E **56**, 5705 (1997).

[15] T. Kajiyama, K. Tanaka, and A. Takahara, Surface molecular motion of the monodisperse polystyrene films, Macromolecules **30**, 280 (1997).

[16] S. Kawana and R. A. L. Jones, Character of the glass transition in thin supported polymer films, Phys. Rev. E **63**, 021501 (2001).

[17] J. Yin and J. A. Forrest, Film thickness dependent stability and glass transition temperature of polymer films produced by physical vapor deposition, Phys. Rev. Lett. **130**, 168101 (2023).

[18] P. A. O'Connell and G. B. McKenna, Rheological measurements of the thermoviscoelastic response of ultrathin polymer films, Science **307**, 1760 (2005).

[19] P. A. O'Connell, S. A. Hutcheson, and G. B. McKenna, Creep behavior of ultra-thin polymer films, J. Polym. Sci. Part B: Polym. Phys. **46**, 1952 (2008).

[20] H.-W. Hu and S. Granick, Viscoelastic dynamics of confined polymer melts, Science **258**, 1339 (1992).

[21] H. Bodiguel and C. Fretigny, Reduced viscosity in thin polymer films, Phys. Rev. Lett. **97**, 266105 (2006).

[22] Z. Yang, Y. Fujii, F. K. Lee, C.-H. Lam, and O. K. C. Tsui, Glass transition dynamics and surface layer mobility in unentangled polystyrene films, Science **328**, 1676 (2010).
[23] J. M. Rathfon, R. W. Cohn, A. J. Crosby, J. P. Rothstein, and G. N. Tew, Confinement effects on chain entanglement in free-standing polystyrene ultrathin films, Macromolecules **44**, 5436 (2011).
[24] Y. Chai, T. Salez, J. D. McGraw, M. Benzaquen, K. Dalnoki-Veress, E. Raphaël, and J. A. Forrest, A direct quantitative measure of surface mobility in a glassy polymer, Science **343**, 994 (2014).
[25] H. D. Rowland, W. P. King, J. B. Pethica, and G. L. W. Cross, Molecular confinement accelerates deformation of entangled polymers during squeeze flow, Science **322**, 720 (2008).
[26] M. Doi and S. F. Edwards, *The Theory of Polymer Dynamics* (Oxford University Press, New York, 1986).
[27] M. Rubinstein and R. H. Colby, *Polymer Physics* (Oxford University Press, New York, 2003).
[28] C. W. Macosko, Joe Starita—father of modern rheometry, Rheol. Bull. **79**, 11 (2010).
[29] T. P. Russell, Polymers find plenty of wiggle room at the bottom, Science **341**, 1351 (2013).
[30] Z. Hao, A. Ghanekarade, N. Zhu, K. Randazzo, D. Kawaguchi, K. Tanaka, X. Wang, D. S. Simmons, R. D. Priestley, and B. Zuo, Mobility gradients yield rubbery surfaces on top of polymer glasses, Nature (London) **596**, 372 (2021).
[31] J. Huang, M. Juszkiewicz, W. H. de Jeu, E. Cerda, T. Emrick, N. Menon, and T. P. Russell, Capillary wrinkling of floating thin polymer films, Science **317**, 650 (2007).
[32] P. Damman, S. Gabriele, S. Coppée, S. Desprez, D. Villers, T. Vilmin, E. Raphaël, M. Hamieh, S. A. Akhrass, and G. Reiter, Relaxation of residual stress and reentanglement of polymers in spin-coated films, Phys. Rev. Lett. **99**, 036101 (2007).
[33] O. Bäumchen, R. Fetzer, and K. Jacobs, Reduced interfacial entanglement density affects the boundary conditions of polymer flow, Phys. Rev. Lett. **103**, 247801 (2009).
[34] G. Reiter, Dewetting of thin polymer films, Phys. Rev. Lett. **68**, 75 (1992).
[35] See Supplemental Material at http://link.aps.org/supplemental/10.1103/PhysRevResearch.7.023226 for the physical characteristics of the samples; $J(t)$ obtained by fitting the ridge profile; expression of k; $h(t)$ of thick polymer films and the correlation with polymer dynamics; expressions of $G'(\omega)$ and $G''(\omega)$, and $G'(\omega)$ and $G''(\omega)$ of PS, PαMS, PtBS, and P4MS derived from the nanorheology technique; description of $G'(\omega)$ and $G''(\omega)$ using the Baumgaertel-Schausberger-Winter model; complex viscosity of PS, PαMS, PtBS, and P4MS; $h(t)$ and the LVE spectra of thin polymer films; thickness and depth dependence of $M_e(\delta)$ and effect of the T_g shift on dynamics of the films.
[36] Q. Wang, W. Wang, C. Wu, J. Luo, J. Zhou, and B. Zuo, Wetting-induced elastocapillary deformation of supported thin rubbery polymer films, Macromolecules **57**, 10112 (2024).
[37] R. W. Style, A. Jagota, C.-Y. Hui, and E. R. Dufresne, Elastocapillarity: Surface tension and the mechanics of soft solids, Annu. Rev. Condens. Matter Phys. **8**, 99 (2017).
[38] J. Bico, É. Reyssat, and B. Roman, Elastocapillarity: When surface tension deforms elastic solids, Annu. Rev. Fluid Mech. **50**, 629 (2018).
[39] B. Andreotti and J. H. Snoeijer, Statics and dynamics of soft wetting, Annu. Rev. Fluid Mech. **52**, 285 (2020).
[40] B. Zhao, E. Bonaccurso, G. K. Auernhammer, and L. Chen, Elasticity-to-capillarity transition in soft substrate deformation, Nano Lett. **21**, 10361 (2021).
[41] R. W. Style, R. Boltyanskiy, Y. Che, J. S. Wettlaufer, L. A. Wilen, and E. R. Dufresne, Universal deformation of soft substrates near a contact line and the direct measurement of solid surface stresses, Phys. Rev. Lett. **110**, 066103 (2013).
[42] A. Carré, J.-C. Gastel, and M. E. R. Shanahan, Viscoelastic effects in the spreading of liquids, Nature (London) **379**, 432 (1996).
[43] R. Pericet-Camara, G. K. Auernhammer, K. Koynov, S. Lorenzoni, R. Raiteri, and E. Bonaccurso, Solid-supported thin elastomer films deformed by microdrops, Soft Matter **5**, 3611 (2009).
[44] E. R. Jerison, Y. Xu, L. A. Wilen, and E. R. Dufresne, Deformation of an elastic substrate by a three-phase contact line, Phys. Rev. Lett. **106**, 186103 (2011).
[45] D. Long, A. Ajdari, and L. Leibler, Static and dynamic wetting properties of thin rubber films, Langmuir **12**, 5221 (1996).
[46] R. W. Style and E. R. Dufresne, Static wetting on deformable substrates, from liquids to soft solids, Soft Matter **8**, 7177 (2012).
[47] M. L. Williams, R. F. Landel, and J. D. Ferry, The temperature dependence of relaxation mechanisms in amorphous polymers and other glass-forming liquids, J. Am. Chem. Soc. **77**, 3701 (1955).
[48] N. W. Tschoegl, *The Phenomenological Theory of Linear Viscoelastic Behavior* (Springer, New York, 1989).
[49] T. G. Mason, Estimating the viscoelastic moduli of complex fluids using the generalized Stokes–Einstein equation, Rheol. Acta **39**, 371 (2000).
[50] S. Hassani, *Mathematical Physics—A Modern Introduction to Its Foundations* (Springer, New York, 1999).
[51] J. K. Jackson, M. E. De Rosa, and H. H. Winter, Molecular weight dependence of relaxation time spectra for the entanglement and flow behavior of monodisperse linear flexible polymers, Macromolecules **27**, 2426 (1994).
[52] R. H. Colby, L. J. Fetters, and W. W. Graessley, The melt viscosity-molecular weight relationship for linear polymers, Macromolecules **20**, 2226 (1987).
[53] P. G. de Gennes, Reptation of a polymer chain in the presence of fixed obstacles, J. Chem. Phys. **55**, 572 (1971).
[54] M. Doi, Explanation for the 3.4-power law for viscosity of polymeric liquids on the basis of the tube model, J. Polym. Sci.: Polym. Phys. Ed. **21**, 667 (1983).
[55] C. W. Macosko, *Rheology—Principles, Measurements, and Applications* (Wiley-VCH, Inc., New York, 1994).
[56] J. des Cloizeaux, Double reptation Vs. simple reptation in polymer melts, Europhys. Lett. **5**, 437 (1988).
[57] A. E. Likhtman and T. C. B. McLeish, Quantitative theory for linear dynamics of linear entangled polymers, Macromolecules **35**, 6332 (2002).
[58] B. Frieberg, E. Glynos, and P. F. Green, Structural relaxations of thin polymer films, Phys. Rev. Lett. **108**, 268304 (2012).
[59] H. R. Brown and T. P. Russell, Entanglements at polymer surfaces and interfaces, Macromolecules **29**, 798 (1996).
[60] A. Silberberg, Distribution of conformations and chain ends near the surface of a melt of linear flexible macromolecules, J. Colloid Interface Sci. **90**, 86 (1982).

[61] L. Si, M. V. Massa, K. Dalnoki-Veress, H. R. Brown, and R. A. L. Jones, Chain entanglement in thin free-standing polymer films, Phys. Rev. Lett. **94**, 127801 (2005).

[62] F. Wang, Z. Jiang, X. Lin, C. Zhang, K. Tanaka, B. Zuo, W. Zhang, and X. Wang, Suppressed chain entanglement induced by thickness of ultrathin polystyrene films, Macromolecules **54**, 3735 (2021).

[63] D. M. Sussman, W.-S. Tung, K. I. Winey, K. S. Schweizer, and R. A. Riggleman, Entanglement reduction and anisotropic chain and primitive path conformations in polymer melts under thin film and cylindrical confinement, Macromolecules **47**, 6462 (2014).

[64] J. H. Kim, J. Jang, and W.-C. Zin, Thickness dependence of the glass transition temperature in thin polymer films, Langmuir **17**, 2703 (2001).